Surrogate-Based Circuit Design Centering

Abdel-Karim S.O. Hassan and Ahmed S.A. Mohamed

Abstract Circuit design centering is one of the most important problems concerning the optimal design of circuits. Circuit design centering seeks nominal values of designable circuit parameters that maximize the probability of satisfying the design specifications (yield function). Design centering can be performed geometrically by finding the center of the feasible region (region in the designable parameter space where the design specifications are satisfied), or by maximizing the yield function explicitly. For all cases, the high expense of circuit simulations required obstructs the design centering process, especially for microwave circuits. To overcome this, computationally cheap surrogate-based models (e.g., space mapping, response surfaces, kriging, and neural networks) can be used for approximating the response functions or the yield function itself. In this chapter the design centering problem is formulated as an optimization problem, and the estimation of the yield function through several sampling techniques is explained. The difficulties facing the design centering process, especially for microwave circuits, are discussed, and the role of surrogate-based models in overcoming these difficulties is demonstrated. Special interest is devoted to space mapping surrogates and microwave circuit design centering. Some of the important surrogate-based circuit design centering approaches are reviewed with an overview of their theoretical bases. Tutorial and practical circuit examples are given to show the effectiveness of these approaches.

Keywords CAD · Design centering · Yield optimization · Surrogate-based optimization · Ellipsoidal technique · Semi-definite programming (SDP) · Trust region optimization · Space-mapping surrogates · EM-based design

A.-K.S.O. Hassan (✉) · A.S.A. Mohamed
Engineering Mathematics and Physics Department, Faculty of Engineering, Cairo University, Giza 12211, Egypt
e-mail: asho_hassan@yahoo.com

A.S.A. Mohamed
e-mail: aashiry@ieee.org

S. Koziel, L. Leifsson (eds.), *Surrogate-Based Modeling and Optimization*,
DOI 10.1007/978-1-4614-7551-4_2,

1 Introduction

In circuit design, circuits are characterized by some designable parameters $\mathbf{x} \in \mathbb{R}^n$ and circuit performance measures $f_i(\mathbf{x})$, $i = 1, 2, \ldots, m$. Designable circuit parameters may be passive elements or transistor geometries. The performance measures may be power dissipation or the circuit S-parameters. Naturally, circuit performance measures are functions of circuit responses which are evaluated through circuit simulations. The desired performance of a circuit (the design specifications) is described by specifying bounds on the performance measures of the circuit which is set by the designer. These design specifications constrain the designable parameters and define a region in the designable parameter space known as the feasible region (design region), which can be defined as:

$$F = \left\{ \mathbf{x} \in \mathbb{R}^n \mid f_i\big(\mathbf{R}(\mathbf{x})\big) \leq b_i,\ i = 1, 2, \ldots, m \right\}, \tag{1}$$

where $\mathbf{x} \in \mathbb{R}^n$ is the vector of the designable parameters, $\mathbf{R} : \mathbb{R}^n \to \mathbb{R}^m$ is the response vector, n is the number of designable parameters, m is the number of constraints, f_i is the i-th performance function, and b_i is the corresponding specification bound. Every $\mathbf{x} \in F$ is considered as an acceptable circuit.

In general, the traditional circuit design trend uses optimization techniques to find a nominal design of the circuit, i.e., to determine the nominal values of circuit parameters which satisfy the design specifications. It is a fact that circuit parameters are subject to known but unavoidable statistical fluctuations inherent to the manufacturing process used, due to environmental effects during operations, or due to model uncertainties. This may cause the circuit performance to violate the design specifications, especially when the location of the nominal design point in the designable parameter space is closer to the boundaries of the feasible region. To simulate the statistical fluctuations, circuit designable parameters are assumed to be random variables with a joint probability density function (PDF) $P(\mathbf{x}, \mathbf{x}_0)$, where $\mathbf{x}_0 \in \mathbb{R}^n$ is the vector of nominal parameter values. Therefore, the probability of satisfying the design specifications (yield function) can be defined as:

$$Y(\mathbf{x}_0) = \int_F P(\mathbf{x}, \mathbf{x}_0)\, dx. \tag{2}$$

The design centering problem seeks nominal values of circuit parameters which minimize the undesirable effects of the statistical fluctuations that affect the designable circuit parameters; namely, it seeks the nominal values of circuit parameters which maximize the yield function. Hence, the design centering or yield maximization problem is formulated as:

$$\max_{\mathbf{x}_0} \quad Y(\mathbf{x}_0). \tag{3}$$

2 Yield Function Estimation and Sampling Techniques

It is clear that the yield integral (2) cannot be evaluated analytically, since it requires the evaluation of an n-dimensional integral over a "non-explicitly defined" region

[31]. Instead, it can be estimated. One of the famous methods used for estimating the yield integral is the Monte Carlo method [41]. To verify this, we define the acceptance index function, $\mathrm{I_a} : \mathbb{R}^n \to \mathbb{R}$, as:

$$\mathrm{I_a}\left(\mathbf{x}^j\right) = \begin{cases} 1 & \text{if } \mathbf{x}^j \in F, \\ 0 & \text{if } \mathbf{x}^j \notin F, \end{cases} \tag{4}$$

where F is the feasible region defined by (1). Then, the yield integral (2) can be rewritten as:

$$Y(\mathbf{x}_0) = \int_{\mathbb{R}^n} \mathrm{I_a}(\mathbf{x}) P(\mathbf{x}, \mathbf{x}_0)\, dx = E\left\{\mathrm{I_a}(\mathbf{x})\right\}, \tag{5}$$

where $E\{\cdot\}$ denotes expectation.

Hence, the yield value at a nominal parameter vector $\mathbf{x}_0$ can be estimated by generating a set of sample points $\mathbf{x}^j$, $j = 1, 2, \ldots, K$ in the designable parameter space using the PDF of designable parameters. The circuit is simulated for each sample point $\mathbf{x}^j$, and the acceptance index function is evaluated. Hence, the yield function at the nominal parameter vector $\mathbf{x}_0$ can be estimated as:

$$Y(\mathbf{x}_0) \approx \frac{1}{K} \sum_{j=1}^{K} \mathrm{I_a}\left(\mathbf{x}^j\right) = \frac{k}{K}, \tag{6}$$

where k is the number of sample points satisfying the design specifications; i.e., the percentage of acceptable circuits gives an estimate of the yield value at $\mathbf{x}_0$. The error in estimating a yield value (the estimation variance) is given by the following formula [34]:

$$V\left(Y(\mathbf{x}_0)\right) \approx \frac{Y(\mathbf{x}_0)(1 - Y(\mathbf{x}_0))}{K - 1}. \tag{7}$$

It is obvious that the estimation variance is inversely proportional to the number of samples considered. Hence, the most straightforward way of improving accuracy and obtaining a low variance estimator is to increase the number of circuit simulations. This can result in prohibitively large requirements for computing time. Furthermore, there is no assurance that all regions of the parameter space will be explored equally well. Several techniques have been proposed for improving the accuracy of a Monte Carlo yield estimate without increasing the number of samples. These methods are called variance reduction techniques [25, 34].

2.1 Variance Reduction Techniques

The main objective of variance reduction techniques is to spread the sample data points as evenly as possible around the interior design space. The benefit is a fewer number of runs, to achieve the same level of confidence, than the number required by the Monte Carlo approach, because it is guaranteed that the entire probability range will be explored.

2.1.1 Importance Sampling

Importance sampling [34] uses another sampling density function in generating the sample points. To compensate this, the values of the acceptance index for sample points are multiplied by weighting factors equal to the ratio between the values of the original PDF and the sampling density function at the sample points. The proper choice of the sampling density function can lead to a variance smaller than that of the standard Monte Carlo yield estimator for the same sample size.

2.1.2 Stratified Monte Carlo Method

The most powerful feature of the Monte Carlo method is the fact that it is the only feasible and reliable method in large dimensions, since the number of required samples does not depend on the number of circuit parameters. The main drawback of the basic Monte Carlo sampling design is that the generated samples may leave large regions of the design region unexplored, as shown in Fig. 1(a) in a 2D case. A modified method to solve this deficiency is the stratified Monte Carlo method, in which stratified sampling is applied [34, 36]. In the stratified Monte Carlo method, each design parameter range is divided into subintervals (bins) of equal probability. A sampling site is then selected within each bin. Figure 1(b) shows an example in the 2D case with a uniform distribution of design variables (four bins for each design variable).

2.1.3 Latin Hypercube Sampling (LHS)

Latin hypercube sampling was developed in the work of McKay et al. [40]. It provides a more accurate estimate of the function value than the Monte Carlo method. The LHS involves dividing the design space into equiprobable subregions. Then N samples are selected such that all subregions are sampled.

One common way to generate N samples using the LHS design is to divide each design variable range into N nonoverlapping equiprobable intervals, each with a probability of $1/N$. Then N different values are selected for each variable at random (one for each interval). This process divides the n-dimensional design space into N^n cells with a probability $1/N^n$ each. The final N samples are obtained by selecting random combinations from the N values of all design variables. Figure 1(c) shows an example of LHS sampling for $n = 2$ design variables and $N = 4$ samples.

3 Circuit Design Centering

Circuit design centering is one of the most important problems concerning the optimal design of circuits [10, 26]. The design centering problem seeks nominal values of circuit parameters which maximize the yield function. Design centering approaches can be classified as statistical approaches and geometrical approaches. Statistical approaches optimize the yield function explicitly using statistical analysis

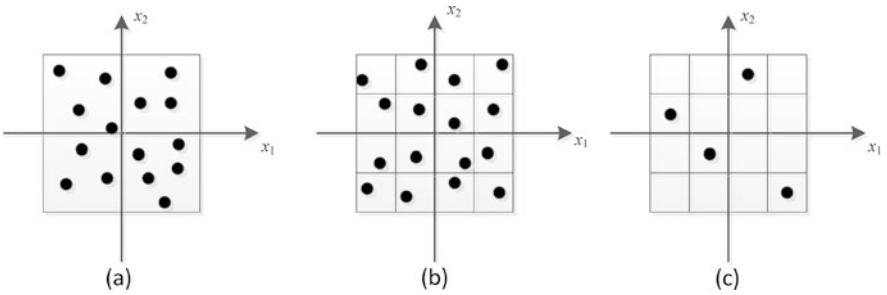

Fig. 1 (**a**) Basic Monte Carlo sampling. (**b**) Stratified Monte Carlo sampling. (**c**) Latin hypercube sampling for two dimensions with $N = 4$

techniques in a straightforward way regardless of the size of the problem or its convexity [23, 31, 32, 35, 36, 49, 53, 59, 60]. As previously stated, the accuracy of the statistical estimation does not depend on the number of parameters and performance features, but on the size of the sample [26]. An acceptable accuracy requires a large number of circuit simulations, in the range of thousands. Hence, the large computational effort required in addition to the uncertainty involved in the estimation process represent an obstacle against the statistical design centering approaches. Geometrical approaches, on the other hand, optimize the yield function implicitly by finding the center of the feasible region. This may be performed by approximating the feasible region using a convex body, e.g., a hyperellipsoid. Then the center of this body is considered as the design center [1–5, 7, 9, 22, 27–30, 33, 46, 48, 57, 58]. The geometrical approaches have fast convergence for convex and small-dimensional problems. Hybrid methods, which combine both approaches, may be used to overcome such problems [33].

4 Surrogate-Based Circuit Design Centering

In general, treating the feasible region during implemention of the geometrical design centering approaches requires evaluating the performance functions and perhaps also evaluating their gradients. Consequently, many circuit simulations will be needed during the design centering process. On the other hand, the statistical design centering process has some permanent special difficulties. For example, the cost of finding a yield value for a given nominal design parameter represents an obstacle for many optimization methods. Hence, robust optimization methods that utilize the fewest possible number of yield evaluations are required. Another difficulty is the absence of any gradient information, as the required simulations cost in evaluating the gradient information is prohibitive in practice [26]. Attempting to approximate the yield gradients using the finite difference approach requires many more yield evaluations, which highly increase the computational cost. Another objection in estimating the gradients by finite differencing is that the estimated yield values are usually contaminated by some numerical noise due to estimation uncertainty. In

these cases, for any small perturbations around a given point, the corresponding yield values do not reflect the local behavior of the yield function itself, but rather that of the noise [31]. Hence, gradient-based optimization methods cannot be applied here.

For all cases of design centering, the high expense of the required circuit simulations may obstruct the design centering process. One of the intelligent methods to overcome this obstacle is to use computationally cheap surrogate-based models. The surrogate-based models may be, for example, space mapping, response surfaces, kriging models, or neural networks. These surrogate-based models can be used for approximating the response functions and the yield function itself. The surrogate-based models are initially constructed and iteratively updated during the design centering process.

4.1 Surrogate-Based Statistical Design Centering Using Trust Region Optimization and Variance Reduction

A surrogate-based statistical design centering algorithm was introduced by Hassan et al. [31] to overcome the difficulties of statistical yield optimization. The algorithm neither requires nor approximates the gradients of the yield and the performance functions. It consists of two parts: a non-derivative unconstrained optimizer and a variance reduction estimator. The first part of the algorithm implements a non-derivative optimization method that combines a trust region framework with quadratic interpolating surrogates for the yield function [18, 19, 43]. The principal operation of the method relies on building, successively updating, and optimizing a quadratic surrogate of the yield function over trust regions. The quadratic surrogate of the yield function reasonably reflects the local behavior of the yield function in a trust region around a current iterate. A new point is then found by maximizing the surrogate model over the trust region. The second part of the algorithm utilizes the stratified Monte Carlo sampling technique [34, 36] for yield estimation during the optimization process. With this sampling technique, a lower variance yield estimator can be obtained which decreases the number of circuit simulations required to achieve a desired accuracy level.

In the given algorithm, the computationally expensive yield function is locally approximated around a current design point $\mathbf{x}_k$ by a computationally cheaper quadratic surrogate model $M(\mathbf{x})$, which can be placed in the form:

$$M(\mathbf{x}) = c + \mathbf{g}^T(\mathbf{x} - \mathbf{x}_k) + \frac{1}{2}(\mathbf{x} - \mathbf{x}_k)^T \mathbf{B}(\mathbf{x} - \mathbf{x}_k), \tag{8}$$

where $c \in \mathbb{R}$, $\mathbf{g} \in \mathbb{R}^n$, and the symmetric matrix $\mathbf{B} \in \mathbb{R}^{n \times n}$ are the unknown parameters of $M(\mathbf{x})$. The total number of these unknowns is $N = \frac{1}{2}(n+1)(n+2)$. These parameters are determined by interpolating the yield function at N interpolation points $\mathbf{x}_i$ using the matching conditions:

$$M(\mathbf{x}_i) = Y(\mathbf{x}_i), \quad i = 1, 2, \ldots, N. \tag{9}$$

However, for $n > 1$, the existence and uniqueness of $M(\mathbf{x})$ are not guaranteed by the number of interpolation points only. Some geometric restrictions on their positions must be satisfied [20, 47]. In other words, if expression (9) is written as a system of linear equations in the unknown parameters of $M(\mathbf{x})$, then the $N \times N$ coefficient matrix of this system (Vandermonde matrix) should be nonsingular for the quadratic interpolating model to be considered as a good approximation of the yield function around $\mathbf{x}_k$. On the other hand, typical distances between the interpolation points are taken to be of the magnitude of a positive scalar denoted ρ [43], which helps to reduce the contribution from the noise to the computations.

Assume that the current design point $\mathbf{x}_k$ in Eq. (8) is chosen to be the interpolation point that provides the best yield value so far, i.e.,

$$Y(\mathbf{x}_k) \geq Y(\mathbf{x}_i), \quad i = 1, 2, \ldots, N. \tag{10}$$

The model $M(\mathbf{s})$ is then maximized, in place of the yield function, over the current trust region and a new point is produced by solving the trust region subproblem:

$$\max_{\mathbf{s} \in \mathbb{R}^n} \quad M(\mathbf{s}) \quad \text{s.t.} \quad \|\mathbf{s}\| \leq \Delta, \tag{11}$$

where $\mathbf{s} = \mathbf{x} - \mathbf{x}_k$, $\Delta \geq \rho$ is the current trust region radius, and $\|\cdot\|$ throughout is the l_2-norm. This problem can be solved by the method of Moré and Sorensen [42]. Let $\mathbf{s}^*$ denote the solution of (11), and then a new point $\mathbf{x}_n = \mathbf{x}_k + \mathbf{s}^*$ is obtained. The ratio between the actual yield increase and the model increase obtained at this point is given by:

$$r = \frac{Y(\mathbf{x}_n) - Y(\mathbf{x}_k)}{M(\mathbf{x}_n) - M(\mathbf{x}_k)}. \tag{12}$$

This ratio reflects how much the surrogate model agrees with the yield function within the trust region. If there is good agreement, i.e., $r \geq 0.7$, the trust region radius Δ is enlarged. However, if the agreement is poor, $r < 0.1$, then Δ is reduced. For moderate r, i.e., $0.1 \leq r < 0.7$, Δ is considered suitable.

The newly obtained information represented in the pair $(\mathbf{x}_n, Y(\mathbf{x}_n))$ is exploited in modifying and improving the quadratic model, if possible. For $Y(\mathbf{x}_n) > Y(\mathbf{x}_k)$, one of the current interpolation points will be dropped and $\mathbf{x}_n$ will be included instead. In this situation, $\mathbf{x}_n$ enters the interpolation point set and a new iteration will then begin by maximizing the improved model over the new trust region. When the point $\mathbf{x}_n$ fails to increase the yield or modify the model, a procedure aims at checking and (possibly) improving the validity of the model around the current point $\mathbf{x}_k$. This procedure eliminates the worst interpolation point, $\mathbf{x}_j$ say, and searches for a new replacing point $\hat{\mathbf{x}}_j$ in the neighborhood $\|\mathbf{x} - \mathbf{x}_k\| \leq \rho$ [43]. The calculations will continue with the current value of ρ if and only if $\|\mathbf{s}^*\| > \rho$, where $\mathbf{s}^*$ is the solution of (11). Otherwise, no more iteration is required for the current value of ρ, since the model is considered valid but it seems that steps of length ρ fail to increase the yield. Hence, ρ is reduced, or termination occurs if either ρ reaches a final value or a prescribed yield increase is achieved.

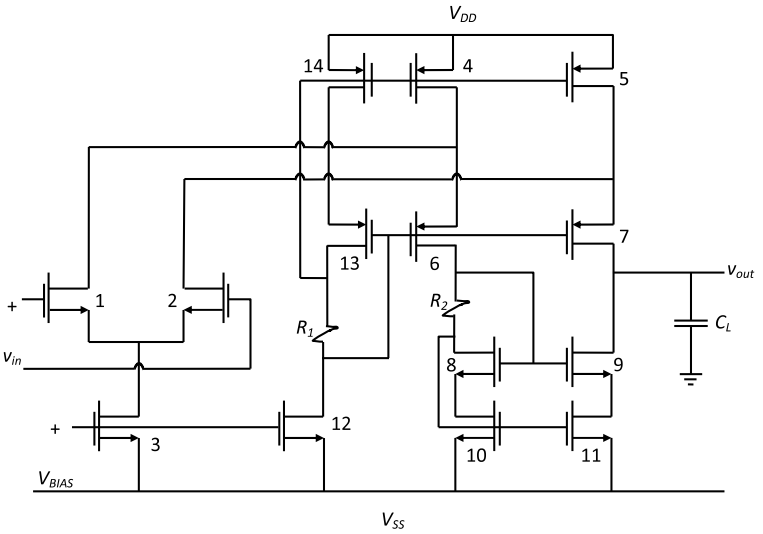

Fig. 2 A folded cascode operational amplifier [6]

Table 1 Performance specifications for the folded cascode operational amplifier [31]

Performance measure	Specification	Initial value	Final value (indep. par)	Final value (correlated parameters)
Slew rate	$\geq$10 V/µs	61	18.07	23.215
Power dissipation	$\leq$10 mW	3.4	0.619	1.0125
Gain bandwidth product	$\geq$10 MHz	49.3	25.6	26.7
Maximum output voltage	$\geq$2 V	1.84	2.177	2.07
Minimum output voltage	≤ -2 V	−1.98	−2.216	−2.157
Maximum input CM voltage	$\geq$2.5 V	2.87	3.028	2.98
Minimum input CM voltage	≤ -1.3 V	−1.28	−1.52	−1.4
Differential voltage gain	$\geq$5,000	4,009	14,266	10,353
Area of designable transistors	$\leq$300 (µm)^2	176	245	260
Minimum channel length	$\geq$0.8 µm	0.8	1.1	0.966
Minimum channel width	$\geq$10 µm	30	21.3	15.05

4.2 Folded Cascode Operational Amplifier Design Centering

The optimal design of a folded cascode operational amplifier [6] is performed using the given algorithm. The amplifier is shown in Fig. 2. This is a 12D problem in which the designable parameters are the widths and lengths of transistors M_1, M_3, M_4, M_6, and M_8 (in micrometers), together with the load capacitor C_L (in picofarads) and the biasing voltage V_{bias} (in volts). There are 11 performance mea-

sures of interest given in Table 1. In this table, the area is defined as the sum of the product of the widths and lengths of all the designable transistors. Table 1 also shows the specification bounds of the performance measures, and their values at the initial and final design parameters. The parameter variance vector is assumed to be $[0.125\ 0.125\ 0.125\ 0.125\ 0.125\ 0.5\ 0.5\ 0.5\ 0.5\ 0.5\ 0.15\ 0.125]^T$ and the maximum cross-correlation coefficient is 0.8. The algorithm starts from a bad initial design $[0.8\ 0.8\ 0.8\ 0.8\ 0.8\ 30.0\ 30.0\ 70.0\ 60.0\ 30.0\ 3.0\ -1.5]^T$ at which the yield is 0.2 %. The algorithm reaches a final design for independent parameters $[1.23\ 1.19\ 1.09\ 1.25\ 1.14\ 29.22\ 25.59\ 69.12\ 59.75\ 5.47\ 1.83\ -1.632]^T$ at which the yield is 92.6 % by using 246 yield evaluations. For the case of correlated parameters, the algorithm reaches the final design center $[1.19\ 1.57\ 1.16\ 1.04\ 1.2\ 30.59\ 23.77\ 70.37\ 65.85\ 30.19\ 2.33\ -2.06]^T$ at which the yield is 93 % by using 259 yield evaluations. A comparison between the stratified sampling and the Monte Carlo method showed that the standard deviation of the stratified sampling yield estimator by using 1,000 samples is almost upper bounded by that of the Monte Carlo estimator by using 1,800 samples, which saves about 44 % of the circuit simulations [31].

The effectiveness of the given algorithm is tested by applying another optimizer for yield maximization. The optimizer uses the Nelder and Mead simplex method with quadratic response surface [24]. After an upper bound of 1,000 yield evaluations, yields of only 12.9 % for independent parameters and 23.5 % for the correlated parameters are obtained.

5 Surrogate-Based Microwave Circuit Design Centering

Design centering of nonlinear microwave circuits is a great challenge [12]. The computational overhead is one of the main difficulties in the design centering process of these circuits, as many full-wave electromagnetic (EM) simulations would be required. For both statistical and geometrical design centering approaches, the high cost of expensive EM circuit simulations required obstructs the design centering process. To overcome this, computationally cheap surrogate-based models can be used for approximating the response functions and the yield function itself.

The problem of high computational cost required for microwave design centering has been solved successfully by using space mapping interpolating surrogates (SMISs) [5, 32]. Space mapping (SM) techniques employ computationally fast, coarse models to greatly reduce the evaluation cost of the computationally expensive full-wave EM fine models [8, 13–15, 17, 37]. The SMIS technique aims to calibrate a space-mapped surrogate, via input and output mappings, to match the fine model with high accuracy.

As previously given, the desired performance of a microwave circuit is described by some performance specifications which define the feasible region in the designable parameter space:

$$F = \left\{ \mathbf{x} \in \mathbb{R}^n \ \mid \ f_i\left(\mathbf{R}_f(\mathbf{x})\right) \ \leq b_i,\ i = 1, 2, \ldots, m \right\}, \tag{13}$$

where $\mathbf{x} \in \mathbb{R}^n$ is the vector of the designable parameters, $\mathbf{R}_f : \mathbb{R}^n \to \mathbb{R}^m$ is the fine model response vector, n is the number of design parameters, m is the number of constraints, f_i is the i-th performance function, and b_i is the corresponding specification bound. However, working with (13) involves a lot of computationally expensive fine model evaluations. Instead, SMISs can be employed, and the feasible region is approximated by:

$$F_s = \left\{ \mathbf{x} \in \mathbb{R}^n \mid f_i\left(\mathbf{R}_s(\mathbf{x})\right) \leq b_i,\ i = 1, 2, \ldots, m \right\}, \tag{14}$$

where F_s is the SM feasible region approximation, and $\mathbf{R}_s : \mathbb{R}^n \to \mathbb{R}^m$ is the SMIS response vector. Two matching conditions have to be satisfied:

$$\mathbf{R}_s(\mathbf{x}) = \mathbf{R}_f(\mathbf{x}), \tag{15}$$

$$\mathbf{J}_s(\mathbf{x}) = \mathbf{J}_f(\mathbf{x}), \tag{16}$$

where $\mathbf{J}_s$ and $\mathbf{J}_f$ are the Jacobian matrices of the surrogate and fine model, respectively. These matrices contain the first-order partial derivatives of the response vector with respect to designable parameters.

5.1 Generalized Space Mapping (GSM) Surrogate Model

The GSM surrogate model is constructed, using a computationally fast coarse model with input and output mappings, in the form [37]:

$$\mathbf{R}_s^i(\mathbf{x}) = \mathbf{A}^i.\mathbf{R}_c\left(\mathbf{B}^i.\mathbf{x} + \mathbf{c}^i\right) + \mathbf{d}^i + \mathbf{E}^i\left(\mathbf{x} - \mathbf{x}_0^i\right), \tag{17}$$

where $\mathbf{x}_0^i$ is the current nominal parameter vector, $\mathbf{A}^i \in M_{m\times m}$ is a diagonal matrix, $\mathbf{R}_c : X_c \to \mathbb{R}^m$ is the coarse model response vector, $\mathbf{B}^i \in M_{n\times n}$, $\mathbf{c}^i \in M_{n\times 1}$, and $\mathbf{d}^i \in M_{m\times 1}$ is given:

$$\mathbf{d}^i = \mathbf{R}_f\left(\mathbf{x}_0^i\right) - \mathbf{A}^i \cdot \mathbf{R}_c\left(\mathbf{B}^i.\mathbf{x}_0^i + \mathbf{c}^i\right), \tag{18}$$

where $\mathbf{R}_f : X_f \to \mathbb{R}^m$ is the fine model response vector, and $\mathbf{E}^i \in \mathrm{M}_{m\times n}$ is

$$\mathbf{E}^i = \mathbf{J}_f\left(\mathbf{x}_0^i\right) - \mathbf{A}^i \cdot \mathbf{J}_c\left(\mathbf{B}^i.\mathbf{x}_0^i + \mathbf{c}^i\right).\mathbf{B}^i, \tag{19}$$

where $\mathbf{J}_f : X_f \to \mathbb{R}^{m\times n}$ and $\mathbf{J}_c : X_c \to \mathbb{R}^{m\times n}$ are the Jacobian matrices of the fine and coarse model responses with respect to the corresponding points, respectively. The mapping parameters $\mathbf{A}^i, \mathbf{B}^i, \mathbf{c}^i$ are obtained by the parameter extraction (PE) optimization process given by:

$$\left(\mathbf{A}^i, \mathbf{B}^i, \mathbf{c}^i\right) = \arg\min_{\mathbf{A},\mathbf{B},\mathbf{c}} \mathbf{e}^i(\mathbf{A}, \mathbf{B}, \mathbf{c}), \tag{20}$$

where $\mathbf{e}^i$ represents the response deviation residual of the surrogate from the fine model and is given by:

$$\mathbf{e}^i(\mathbf{A},\mathbf{B},\mathbf{c}) = \sum_{k=0}^{i} w_k \left\| \mathbf{R}_f\left(\mathbf{x}^k\right) - \mathbf{A}\cdot\mathbf{R}_c\left(\mathbf{B}.\mathbf{x}^k + \mathbf{c}\right)\right\| + \sum_{k=0}^{i} v_k \left\| \mathbf{J}_f\left(\mathbf{x}^k\right) - \mathbf{A}\cdot\mathbf{J}_c\left(\mathbf{B}.\mathbf{x}^k + \mathbf{c}\right).\mathbf{B}\right\|, \quad (21)$$

where the coefficients w_k and v_k are chosen according to the nature of the design problem.

5.2 *The Ellipsoidal Technique for Design Centering of Microwave Circuits*

In this work, a SM technique is integrated with an ellipsoidal technique to obtain a surrogate-based geometrical design centering method of microwave circuits with a small number of EM simulations [5]. The ellipsoidal technique [2, 3] approximates the feasible region with a hyperellipsoid which is the final hyperellipsoid of a generated sequence of decreasing volume of different shape and center hyperellipsoids. The center of this final hyperellipsoid is considered as a design center. The generation of the sequence of hyperellipsoids requires successive linearization of the feasible region boundaries at selected boundary points. This requires evaluating the performance functions and their gradients. Consequently, many expensive circuit simulations will be needed, especially for microwave circuits.

In this design centering method, an SMIS [14] is initially constructed and then updated through SM iterations. In each SM iteration, a current SMIS model and the corresponding SM feasible region approximation (14) are available. The ellipsoidal technique is implemented with the current feasible region approximation to obtain a new design centering point. This new center is validated by the fine model and is used to update the current SMIS model. Enhanced improvement is achieved by satisfying (15) at all preceding design centering points (global matching). The ellipsoidal technique is then restarted with the updated SMIS to get the next center. The process is repeated until a final design center is obtained.

5.2.1 The Ellipsoidal Technique

Assume that $\mathbf{x}_0^k$ is the design center obtained in the $(k-1)$-th SM iteration. In the k-th iteration, the feasible region approximation is $F_s^k = \{\mathbf{x} \in \mathbb{R}^n \mid f_i(\mathbf{R}_s^k(\mathbf{x})) \leq b_i, i = 1, 2, \ldots, m\}$. The ellipsoidal technique starts with a sufficiently large hyperellipsoid containing the feasible region approximation with an initial center $\mathbf{t}_0 = \mathbf{x}_0^k$. An iteration of the ellipsoidal technique assumes that the current hyperellipsoid is $\mathbf{E}_j = \{(\mathbf{x}-\mathbf{t}_j)^T \mathbf{Q}_j^{-1}(\mathbf{x}-\mathbf{t}_j) \leq 1\}$ with center $\mathbf{t}_j$ and hyperellipsoid matrix $\mathbf{Q}_j$ which is symmetric and positive definite. A hyperplane $\mathbf{a}^T\mathbf{x} = b$ is then constructed by linearizing the feasible region boundary at a selected boundary point. This hyperplane

divides the current hyperellipsoid into two parts. The first is completely infeasible, while the second contains the feasible region approximation. The new generated hyperellipsoid $\mathbf{E}_{j+1}(\mathbf{t}_{j+1}, \mathbf{Q}_{j+1})$ is the minimum volume hyperellipsoid enclosing the second part with center and matrix given by:

$$\mathbf{t}_{j+1} = \mathbf{t}_j - \eta \frac{(\mathbf{Q}_j \mathbf{a})}{\sqrt{\mathbf{a}^T \mathbf{Q}_j \mathbf{a}}}, \qquad \mathbf{Q}_{j+1} = \beta \left(\mathbf{Q}_j - \gamma \frac{(\mathbf{Q}_j \mathbf{a})(\mathbf{Q}_j \mathbf{a})^T}{\mathbf{a}^T \mathbf{Q}_j \mathbf{a}} \right), \tag{22}$$

where

$$\begin{aligned} &\eta = (1 + n\delta)/(n+1), \qquad \beta = n^2\big(1 - \delta^2\big)/\big(n^2 - 1\big), \\ &\gamma = 2\eta/(1+\delta) \quad \text{and} \quad \delta = \big(\mathbf{a}^T \mathbf{t}_j - b\big)/\sqrt{\mathbf{a}^T \mathbf{Q}_j \mathbf{a}}. \end{aligned} \tag{23}$$

The volumes of $\mathbf{E}_{j+1}$ and $\mathbf{E}_j$ satisfy the ratio [2]:

$$\rho = \rho_0 \big(1 - \delta^2\big)^{\frac{(n-1)}{2}} (1 - \delta), \quad \rho_0 = \frac{(n^n)}{((n+1)^{\frac{(n+1)}{2}} (n-1)^{\frac{(n-1)}{2}})}. \tag{24}$$

The hyperellipsoid volume ratio ρ is a monotonically decreasing function in δ. Thus, different strategies are used to locate the best boundary points, which are accompanied by maximum values of δ. This results in the greatest reduction in the volume of the generated hyperellipsoids and consequently increases the convergence of the ellipsoidal technique [3].

The iterations of the ellipsoidal technique continue until no significant reduction in the hyperellipsoid volume can be achieved. The center of the final hyperellipsoid, denoted by $\mathbf{t}_{\text{final}}$, considers the next design center $\mathbf{x}_0^{k+1}$ and is fed into the next SM iteration [5].

Note that the Broyden formula [16] offers a fast way to approximate the gradients required in linearization. However, for some models, exact gradients can be evaluated by the adjoint sensitivity technique [11, 50].

5.2.2 Design Centering of Coupled-Line Bandpass Filter

The optimal design of a coupled-line bandpass filter [52], shown in Fig. 3, is determined. The design constraint functions are given by:

$$f_i\big(\mathbf{R}_f(\mathbf{x})\big) = \begin{cases} R_{f,i}(\mathbf{x}) + 20, & 5 \text{ GHz} < \omega_i < 7.25 \text{ GHz} \\ -3 - R_{f,i}(\mathbf{x}), & 7.75 \text{ GHz} < \omega_i < 8.25 \text{ GHz} \\ R_{f,i}(\mathbf{x}) + 20, & 8.75 \text{ GHz} < \omega_i < 11 \text{ GHz} \end{cases}$$

where $R_{f,i}(\mathbf{x}) = |S_{21}|$ (dB) at frequency ω_i. The substrate thickness is taken as 1.272 mm and $\varepsilon_r = 10$. The design parameters are $[\,x_1\ x_2\ x_3\ x_4\ x_5\ x_6\,]^T$ in millimeters, as shown in Fig. 3. The simulation of this example is performed using an in-house planar solver based on the method of moments [51]. The fine model is meshed with 3 width and 15 length segments of the microstrip lines, while the coarse model is meshed with 1 width and 5 length segments.

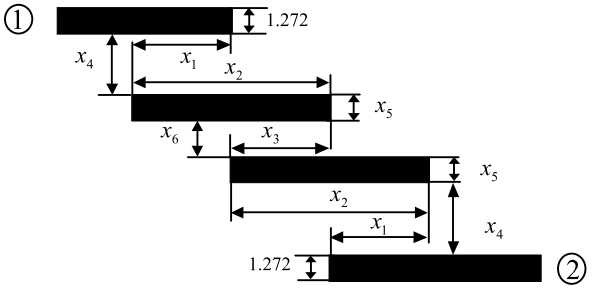

Fig. 3 Coupled-line bandpass filter [52]

Table 2 Yield results for the coupled line bandpass filter assuming independent parameters [5]

Parameter spreads σ	Initial yield	Yield at minimax solution	Final yield
$\sigma_i = 2\ \%$[a]	2 %	5 %	14 %
$\sigma_i = 1\ \%$[a]	0 %	20 %	34 %
$\sigma_i = 0.5\ \%$[a]	0 %	37 %	55 %
$\sigma_i = 0.1019$[b]	0 %	6 %	17 %
$\sigma_i = 0.034$[b]	0 %	45 %	75 %

[a]Parameter spreads are relative to the nominal values at the final solution

[b]Absolute parameter spreads in millimeters

Table 3 Yield results for the coupled-line bandpass filter assuming correlated parameters [5]

Covariance matrix	Initial yield	Yield at minimax solution	Final yield
$\mathbf{Cov}_1$	0 %	10 %	27 %
$\mathbf{Cov}_2$	0 %	57 %	93 %

The constraint functions are evaluated at all frequency points $\omega_i = 5$, 5.75, 6.5, 7.25, 7.75, 8, 8.25, 8.75, 9.5, 10.25, 11 GHz. The initial surrogate is taken as the coarse model giving $[5.682\ 13.991\ 6.835\ 0.522\ 1.051\ 1.511]^T$ as the initial fine model design. The final design center $[5.298\ 12.960\ 6.052\ 0.416\ 2.122\ 1.099]^T$ is reached after six SM iterations. The initial and the final yield values are evaluated via the Monte Carlo method with 100 sample points assuming normally distributed parameters. The results assuming independent parameters are shown in Table 2.

The results for the correlated parameters are shown in Table 3. A much higher yield is achieved with the obtained design center in comparison with the minimax center $[4.779\ 13.664\ 6.835\ 0.637\ 1.024\ 0.808]^T$. In Table 3, $\mathbf{Cov}_1$ and, $\mathbf{Cov}_2$ are final hyperellipsoid matrices scaled to give hyperellipsoids of the same volume as the hyperellipsoids with independent parameter spreads $\sigma_i = 0.1019$ and $\sigma_i = 0.034$.

5.3 Design Centering of Microwave Circuits via Trust Region Optimization and Space Mapping Surrogates

This approach of design centering is a statistical one and treats two types of surrogates [32]. It employs the GSM surrogate (17), to minimize the required expensive EM simulations, in addition to the quadratic surrogate model (8) to approximate the computationally expensive yield function. The approach integrates three strategies to overcome the statistical microwave design centering difficulties. First, Latin hypercube sampling (LHS) is used in the sampling process. Second, a derivative-free trust region method is utilized in the yield optimization process. In the given approach, the NEWUOA algorithm developed by Powell is used [44, 45, 61]. The NEWUOA algorithm employs quadratic surrogate models to approximate the expensive yield function. Third, the GSM technique [37] is employed to reduce the simulation computational effort. Thus, the NEWUOA algorithm is combined with the GSM technique and the LHS technique to obtain a method for statistical microwave circuit design centering.

Starting from an initial point, the GSM surrogate model is initially constructed, and then updated through SM iterations. In each SM iteration, a current SMIS model and the corresponding SM feasible region approximation are available. The NEWUOA algorithm is applied to optimize the yield function and get a better center point. The yield values are estimated using the current feasible region approximation. The new center point is validated by the fine model and is used to update the current SMIS using the matching conditions. Then, the NEWUOA algorithm starts again with the updated surrogate to obtain the next center point.

5.3.1 NEWUOA Algorithm

In the NEWUOA algorithm, the computationally expensive yield function is locally approximated around a current iterate utilizing the quadratic surrogate model $M(\mathbf{x})$ in (8) by interpolating the yield function at $m = 2n + 1$ points. The total number of unknown parameters in the surrogate quadratic model is $N = ½(n + 1)(n + 2)$. The freedom in $M(\mathbf{x})$ is taken up by minimizing the Frobenius norm of the change in the Hessian matrix $\mathbf{B}$ during the optimization process, i.e., $\|\mathbf{B}^{\text{new}} - \mathbf{B}^{\text{old}}\|_F$ [44]. The estimated yield function values are submitted to the optimizer by a subroutine that employs the LHS technique, and the generated samples are tested against the current feasible region approximation.

The quadratic model in (8) is then maximized, instead of the yield function, over a current trust region (TR) by solving the TR subproblem (11). The TR radius is revised according to the agreement between the quadratic model and the yield function at the new point. The TR radius Δ has a lower bound ρ in the interval $[\rho_{\text{fin}}, \rho_{\text{ini}}]$. This parameter ρ is utilized to maintain enough distances between the interpolation points where ρ_{ini} and ρ_{fin} are user-defined initial and final radii, respectively. Let Δ_{old} and Δ_{new} be the old and new values of Δ. The choice of Δ_{new} depends on the ratio between the actual yield increase and the model increase as in (12), and

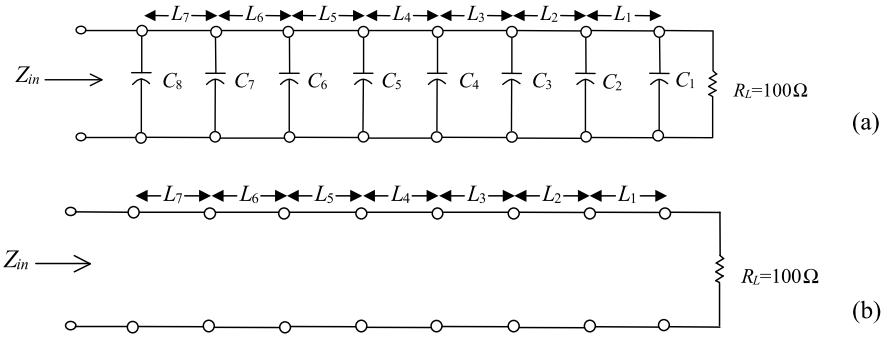

Fig. 4 Seven-section capacitively loaded impedance transformer: (**a**) fine model, (**b**) coarse model

the Euclidean length of the step **s** obtained when solving (11). NEWUOA sets Δ_{new} to ρ or to Δ_{int} when $\Delta_{\text{int}} < 1.5\rho$ or $\Delta_{\text{int}} > 1.5\rho$, respectively, where Δ_{int} is the intermediate value [45]:

$$\Delta_{\text{int}} = \begin{cases} \|\mathbf{s}\|, & r \le 0.1 \\ \max\{\|\mathbf{s}\|,\ 0.5\ \Delta_{\text{old}}\}, & 0.1 < r \le 0.7 \\ \max\{\|\mathbf{s}\|, \Delta_{\text{old}}\}, & r > 0.7 \end{cases} \tag{25}$$

The algorithm is terminated when the TR radius reaches the lower bound ρ_{fin} that fixes the final accuracy required in the parameters [44, 45]. Numerically, NEWUOA shows good results and acceptable accuracy in problems with dimensions up to 320 variables [45].

5.3.2 Design Centering of Seven-Section Transmission Line Capacitively Loaded Impedance Transformer

The seven-section transmission line (TL) capacitively loaded impedance transformer is described in [8]. The coarse model is considered as an ideal seven-section TL, where the "fine" model is a capacitively loaded TL with capacitors $C_1 = \cdots = C_8 = 0.025$ pF (see Fig. 4). The design parameters are $\mathbf{x} = [L_1\ L_2\ L_3\ L_4\ L_5\ L_6\ L_7]^T$, which are the normalized lengths with respect to the quarter-wavelength L_{q} at the center frequency 4.35 GHz. The design specifications are:

$$f_i\left(\mathbf{R}_f(\mathbf{x})\right) = \left|\mathbf{S}_{11}(\mathbf{x}, \omega_i)\right| \le 0.07, \quad 1\ \text{GHz} \le \omega_i \le 7.7\ \text{GHz}$$

with 68 points per frequency sweep.

An initial infeasible point $[0.892\ 0.993\ 0.989\ 0.981\ 0.996\ 0.99\ 0.891]^T$ is considered. The yield values are estimated via the LHS method with 200 sample points assuming normally distributed parameters with covariance matrices G/49 and G/441, where $[0.193\ 0.194\ 0.145\ 0.046\ 0.155\ 0.239\ 0.38]^T$ is a parameter variance vector of the covariance matrix G with maximum cross-correlation coefficient 0.15.

Table 4 Results of the seven-section TL transformer with normally distributed correlated parameters

Covariance matrix	Initial yield		Final yield	
	Surrogate	Fine	Surrogate	Fine
G/49	2.5 %	3.0 %	30.0 %	27.5 %
G/441	0.2 %	0.2 %	99.2 %	100 %

The technique needed three SM iterations to obtain the results shown in Table 4. The yield results at the initial and final designs are shown in Fig. 5.

5.4 Microwave Design Centering via Semidefinite Programming and Space Mapping Surrogates

The method has a statistical-geometrical nature [33]. It exploits semidefinite programming [21, 54–56] and GSM surrogates [37] to approximate the feasible region with two bounding ellipsoids. The centers of these ellipsoids are used as design centers. The bounding ellipsoids are obtained using a two-phase algorithm. In the first phase, the minimum volume ellipsoid enclosing the feasible region is obtained, while the largest ellipsoid that can be inscribed within the feasible region is obtained in the second phase.

5.4.1 Phase (I): Minimum Volume Ellipsoid Enclosing the Feasible Region

The first phase of the method starts with an initial point and an initial GSM surrogate model. This surrogate model is iteratively updated through SM iterations. In each SM iteration a current feasible region approximation is available and a convergent sequence of increasing-volume Löwner–John ellipsoids is generated [21]. The

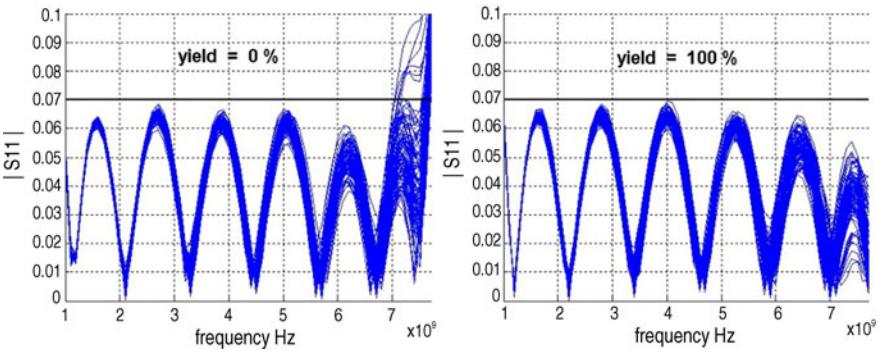

Fig. 5 Yield evaluated at the initial and final design parameter vectors with 100 sample points with covariance matrix G/441 for the seven-section capacitively loaded impedance transformer

generated ellipsoids enclose tightly selected sets of feasible points out of generated sample points. The generated sequence of Löwner–John ellipsoids converges to the minimum volume ellipsoid enclosing the current feasible region approximation, and its center is considered as a design center point. This new point is used to update the current GSM surrogate model using matching conditions. Consequently, a new updated feasible region approximation is constructed, and the process is repeated until the minimum volume ellipsoid is obtained.

Assume that $\mathbf{x}_0^k$ is the design center obtained in the $(k-1)$-th SM iteration. In the k-th iteration, the current feasible region approximation is $F_s^k = \{\mathbf{x} \in \mathbb{R}^n \mid f_i(\mathbf{R}_s^k(\mathbf{x})) \le b_i,\ i = 1, 2, \ldots, m\}$. In the k-th SM iteration, the initial point $\mathbf{q}_{\text{init}} = \mathbf{x}_0^k$ and an initial covariance matrix $\mathbf{B}_{\text{init}}$ are used to generate an LHS normally distributed sample set $\mathrm{S}^{(0)}$. Circuit simulation is executed on the sample set $\mathrm{S}^{(0)}$ in order to determine the feasible points and find the feasible set $\mathrm{S}_f^{(0)} = \mathrm{S}^{(0)} \cap F_s^k$. Then, the minimum volume ellipsoid $\mathcal{E}_{\text{Min}}^{(0)}(\mathbf{q}_{\text{min}}^{(0)}, \mathbf{B}_{\text{min}}^{(0)})$ enclosing the feasible set $\mathrm{S}_f^{(0)}$ (Löwner–John ellipsoid) is constructed as follows.

Let $\mathrm{S}_f^{(0)} = \{\mathbf{z}_1, \mathbf{z}_2, \ldots, \mathbf{z}_p\} \subset \mathbb{R}^n$. Define the ellipsoid,

$$\mathcal{E}(\mathbf{q}, \mathbf{B}) = \left\{\mathbf{z} \in \mathbb{R}^n : (\mathbf{z} - \mathbf{q})^T \mathbf{B}^{-1} (\mathbf{z} - \mathbf{q}) \le \mathbf{1}\right\}, \tag{26}$$

where $\mathbf{q} \in \mathbb{R}^n$ is the center of the ellipsoid, and $\mathbf{B} \in \mathbf{SR}^n, \mathrm{B} \succ 0$ (symmetric and positive definite). Assume that $\mathbf{B} = \mathbf{Q}\mathbf{Q}^T$, where $\mathbf{Q}$ is nonsingular. Without loss of generality, it can be assumed that $\mathbf{Q} \in \mathbf{SR}^n, \mathbf{Q} \succ 0$ [28].

Hence, the minimum volume ellipsoid $\mathcal{E}_{\text{Min}}^{(0)}(\mathbf{q}_{\text{min}}^{(0)}, \mathbf{B}_{\text{min}}^{(0)})$ enclosing the set $S_f^{(0)}$ can be obtained by solving the following determinant maximization problem [54–56]:

$$\begin{aligned} \max \quad & \log\det \mathbf{A}_0 \\ \text{subject to} \quad & \begin{pmatrix} \mathbf{I}_n & \mathbf{A}_0\mathbf{z}_j + \mathbf{b}_0 \\ (\mathbf{A}_0\mathbf{z}_j + \mathbf{b}_0)^T & \mathbf{1} \end{pmatrix} \succcurlyeq \mathbf{0}, \quad j = 1, 2, \ldots, p, \\ & \mathbf{A}_0 = \mathbf{A}_0^T, \quad \mathbf{A}_0 \succ \mathbf{0}, \end{aligned} \tag{27}$$

where $\mathbf{I}_n$ is the n-dimensional identity matrix, $\mathbf{A}_0 = \mathbf{Q}_{\text{min}}^{(0)-\mathbf{1}}$, $\mathbf{b}_0 = -\mathbf{Q}_{\text{min}}^{(0)-\mathbf{1}}\mathbf{q}_{\text{min}}^{(0)}$,

This problem can be solved using semidefinite programming techniques [21, 54]. Clearly, obtaining the optimization variables $\mathbf{b}_0$ and $\mathbf{A}_0$ characterizes the Löwner–John ellipsoid $\mathcal{E}_{\text{Min}}^{(0)}(\mathbf{q}_{\text{min}}^{(0)}, \mathbf{B}_{\text{min}}^{(0)})$. The most distant feasible samples of $S_f^{(0)}$, which carry the dominant information about the ellipsoid $\mathcal{E}_{\text{Min}}^{(0)}$, are drawn into a new set S_{shell},

$$S_{\text{shell}} = \left\{\mathbf{z} \in S_f^{(0)} : r_{\text{shell}}^2 \le \left(\mathbf{z} - \mathbf{q}_{\text{min}}^{(0)}\right)^T \mathbf{B}_{\text{min}}^{(0)-\mathbf{1}} \left(\mathbf{z} - \mathbf{q}_{\text{min}}^{(0)}\right) \le 1\right\}, \tag{28}$$

where $0 \le r_{\text{shell}} \le 0.98$.

Using $\mathbf{q}_{\text{min}}^{(0)}$ and $\mathbf{B}_{\text{min}}^{(0)}$, a generation of LHS normally distributed sample set $S^{(1)}$ is performed. All the new samples of $S^{(1)}$ falling inside the current Löwner–John

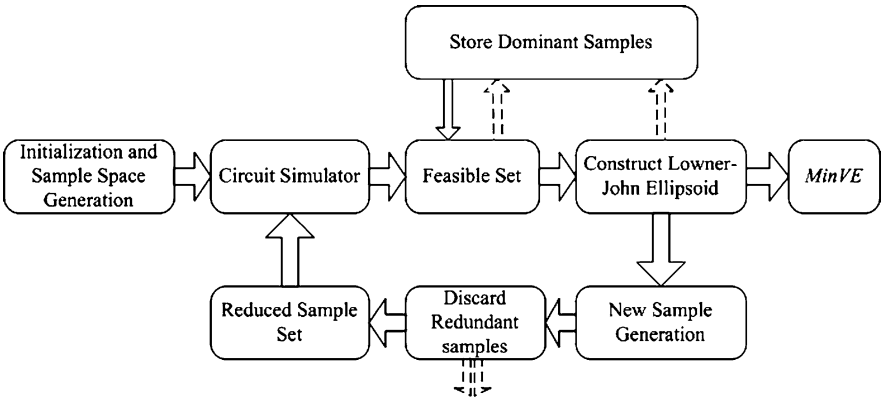

Fig. 6 Block diagram for SM iteration of phase (I) [33]

ellipsoid $\mathcal{E}^{(0)}_{\text{Min}}(\mathbf{q}^{(0)}_{\text{min}}, \mathbf{B}^{(0)}_{\text{min}})$, or a reduced version of it, are deleted, and a reduced sample set S_{reduced} is constructed for $0.9 \leq r_{\text{discard}} \leq 1$ as:

$$S_{\text{reduced}} = \left\{ \mathbf{z} \in \mathbf{S}^{(1)} : \left(\mathbf{z} - \mathbf{q}^{(0)}_{\text{min}}\right)^T \mathbf{B}^{(0)-1}_{\text{min}} \left(\mathbf{z} - \mathbf{q}^{(0)}_{\text{min}}\right) \geq r^2_{\text{discard}} \right\}. \tag{29}$$

Circuit simulation is performed on the reduced sample set S_{reduced}, giving a feasible set $S_f = S_{\text{reduced}} \cap F^k_s$. The stored feasible samples in the set S_{shell} (28) are retrieved and added to the new feasible points of S_f, giving the first iteration's feasible set $S^{(1)}_f = S_f \cup S_{\text{shell}}$. Then, a new Löwner–John ellipsoid $\mathcal{E}^{(1)}_{\text{Min}}(\mathbf{q}^{(1)}_{\text{min}}, \mathbf{B}^{(1)}_{\text{min}})$ can be constructed using the feasible set $S^{(1)}_f$. Since the feasible set $S^{(1)}_f$ carries information about the last Löwner–John ellipsoid, an increased volume ellipsoid is attained, and the convergence of the method is guaranteed. Note that the reduced sample set S_{reduced} saves about 50–60 % of the required circuit simulations if the set $S^{(1)}$ was considered completely [33].

By repeating this process, a sequence of increasing-volume Löwner–John ellipsoids is generated to enclose the current feasible region approximation F^k_s. A suitable stopping criterion is chosen such that the minimum volume ellipsoid $\mathcal{E}_{\text{MinVE}}$ enclosing F^k_s is reached. The center of this ellipsoid is used to update the current GSM surrogate model using matching conditions. Consequently, a new updated feasible region approximation is constructed, and the process is repeated until the minimum volume ellipsoid $\mathcal{E}_{\text{MinVE}}$ enclosing the feasible region is obtained; its center is considered as a design center. Figure 6 shows an SM iteration of phase (I).

5.4.2 Phase (II): Maximum Volume Inscribed Ellipsoid

The second phase of the method treats the final SM feasible region approximation obtained in phase (I). It begins by constructing an initial polytope P_0 containing the minimum volume ellipsoid $\mathcal{E}_{\text{MinVE}}$. The initial polytope hyperplanes are chosen perpendicular to the ellipsoid axes, and passing through their end points. The

initial maximum volume ellipsoid $\mathcal{E}^{(0)}_{\text{Max}}(\mathbf{q}^{(0)}_{\text{max}}, \mathbf{B}^{(0)}_{\text{max}})$ inscribed in the polytope P_0 is the minimum volume ellipsoid $\mathcal{E}_{\text{MinVE}}$ containing the feasible region. An updated polytope P_1 is constructed by adding new hyperplanes obtained by linearizing the feasible region boundaries at selected boundary points. These points are obtained by searching along orthogonal directions, e.g., the parameter directions and/or the current ellipsoid axes, starting from the current ellipsoid's center.

An ellipsoid in $\mathbb{R}^n$ can be defined as [28]:

$$\mathcal{E}(\mathbf{q}, \mathbf{Q}) = \left\{\mathbf{x} \in \mathbb{R}^n : \mathbf{x} = \mathbf{q} + \mathbf{Q}\mathbf{s} \text{ and } \|\mathbf{s}\| \leq 1\right\} \tag{30}$$

where $\mathbf{q} \in \mathbb{R}^n$ is the center, $\mathbf{Q} \in \text{SR}^n$. Assume that the polytope P_1 is given by:

$$\text{P}_1 = \left\{\mathbf{x} \in \mathbb{R}^n : \mathbf{A}\mathbf{x} \leq \mathbf{b}\right\}, \tag{31}$$

where $\mathbf{A} \in \mathbb{R}^{m \times n}$, $m > n$, $\mathbf{b} \in \mathbb{R}^m$. Then, $\mathcal{E}^{(1)}_{\text{Max}}(\mathbf{q}^{(1)}_{\text{max}}, \mathbf{Q}^{(1)}_{\text{max}})$ inscribed within this polytope can be obtained by solving the following problem:

$$\begin{aligned} &\max \quad \log\det \mathbf{Q}^{(1)}_{\text{max}} \\ &\text{S.t.} \quad \begin{pmatrix} (b_j - \mathbf{A}_j^T \mathbf{q}^{(1)}_{\text{max}})\mathbf{I}_n & \mathbf{Q}^{(1)}_{\text{max}}\mathbf{A}_j \\ \mathbf{A}_j^T \mathbf{Q}^{(1)}_{\text{max}} & (b_j - \mathbf{A}_j^T \mathbf{q}^{(\mathbf{1})}_{\text{max}}) \end{pmatrix} \succcurlyeq \mathbf{0}, \quad j = 1, 2, \ldots, m, \\ &\qquad \mathbf{Q}^{(1)}_{\text{max}} = \mathbf{Q}^{(1)T}_{\text{max}}, \qquad \mathbf{Q}^{(1)}_{\text{max}} \succ \mathbf{0}, \end{aligned} \tag{32}$$

where $\mathbf{A}_j^T$ is the j-th row of $\mathbf{A}$, and b_j is the j-th element of $\mathbf{b}$.

Proceeding with the last problem similarly to problem (27), both the ellipsoid center $\mathbf{q}^{(1)}_{\text{max}}$ and the ellipsoid matrix $\mathbf{B}^{(1)}_{\text{max}} = \mathbf{Q}^{(1)}_{\text{max}}\mathbf{Q}^{(1)T}_{\text{max}}$ can be obtained; hence the ellipsoid $\mathcal{E}^{(1)}_{\text{Max}}(\mathbf{q}^{(1)}_{\text{max}}, \mathbf{B}^{(1)}_{\text{max}})$ is obtained.

The previously stated two steps: polytope updating and maximum volume inscribed ellipsoid forming, are repeated until a suitable stopping criterion occurs. Hence, a polytope approximation for the feasible region, attached with the maximum volume ellipsoid $\mathcal{E}_{\text{MaxVE}}$ inscribed within this polytope, is obtained. Consequently, the maximum volume inscribed ellipsoid in the feasible region is obtained.

5.4.3 Design Centering of Six-Section H-Plane Waveguide Filter

The given method is applied for design centering of a six-section H-plane waveguide filter [39]. A waveguide with a width of 3.485 cm is used. The propagation mode is TE_{10} with a cutoff frequency of 4.3 GHz. The six-waveguide sections are separated by seven H-plane septa (as shown in Fig. 7) which have a finite thickness of 0.6223 mm. The design parameters $\mathbf{x}$ are the three waveguide section lengths L_1, L_2, and L_3 and the septa widths W_1, W_2, W_3, and W_4. The feasible region is constrained by the magnitude of the reflection coefficients $|S_{11}|$ at 44 frequency points $\{5.2, 5.3, \ldots, 9.5 \text{ GHz}\}$ as:

$$f_i\left(\mathbf{R}_f(\mathbf{x})\right) = \begin{cases} |S_{11}(\mathbf{x}, \omega_i)| \geq 0.85, & \omega_i \leq 5.2 \text{ GHz} \\ |S_{11}(\mathbf{x}, \omega_i)| \leq 0.16, & 5.4 \text{ GHz} \leq \omega_i \leq 9.0 \text{ GHz} \\ |S_{11}(\mathbf{x}, \omega_i)| \geq 0.5, & \omega_i \geq 9.5 \text{ GHz} \end{cases}$$

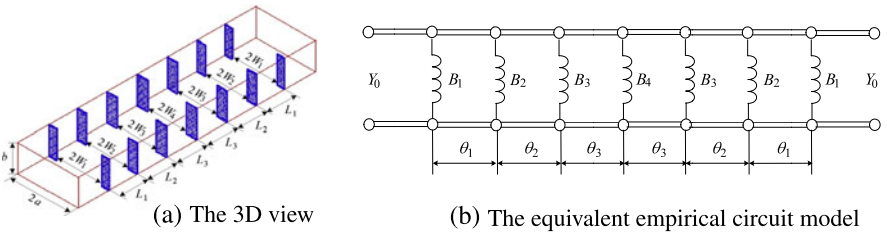

(a) The 3D view (b) The equivalent empirical circuit model

Fig. 7 The six-section H-plane waveguide filter

Table 5 Yield results for correlated parameter case

Covariance matrix	Initial yield	Final yield					
		Actual region		MinVE Approx.		MaxVE Approx.	
		q_{MinVE}	q_{MaxVE}	q_{MinVE}	q_{MaxVE}	q_{MinVE}	q_{MaxVE}
$\mathbf{B}_{\text{MinVE}}/49$	0 %	93 %	94 %	100 %	100 %	54 %	58 %
$\mathbf{B}_{\text{MaxVE}}/16$	0 %	100 %	100 %	100 %	100 %	92 %	96 %

Table 6 Yield results for independent parameter case

Parameter spreads	Initial yield	Final yield					
		Actual region		MinVE Approx.		MaxVE Approx.	
		q_{MinVE}	q_{MaxVE}	q_{MinVE}	q_{MaxVE}	q_{MinVE}	q_{MaxVE}
σ[a]	0 %	71 %	68 %	99 %	99 %	32 %	35 %
$\sigma/2$	0 %	99 %	97 %	100 %	100 %	87 %	93 %

[a] $\boldsymbol{\sigma} = 10^{-4}[0.762889\ 0.766507\ 0.797684\ 0.632623\ 0.584962\ 0.558823\ 0.551575]^T$

An empirical coarse model due to Marcuvitz [38], with lumped inductances and dispersive transmission line sections, is utilized. The simulation of the fine model is performed using High Frequency Structure Simulator (HFSS), starting with the point $\mathbf{x}_0 = 10^{-4}[160\ 160\ 165\ 135\ 120\ 115\ 115]^T$ mm with $\mathbf{B}_{\text{ini}} = 10^{-4} \times \text{I}_7$. Two SM iterations are needed to obtain the following two design centers:

$$\mathbf{q}_{\text{MinVE}} = 10^{-4}[159.703\ 161.876\ 165.426\ 134.022\ 122.086\ 116.969\ 115.662]^T,$$

$$\mathbf{q}_{\text{MaxVE}} = 10^{-4}[159.099\ 161.617\ 165.495\ 134.243\ 121.954\ 117.122\ 115.561]^T$$

The yield values are evaluated at $\mathbf{q}_{\text{init}}$, $\mathbf{q}_{\text{MinVE}}$ and $\mathbf{q}_{\text{MaxVE}}$ via the Monte Carlo method using 100 normally distributed samples for each yield evaluation. Tables 5 and 6 show the results for the correlated and independent cases, respectively.

Acknowledgements The authors would like to thank Prof. Slawomir Koziel, School of Science and Engineering, Reykjavik University, for his invitation to contribute to this book. The authors also would like to acknowledge the contributions to the original work by Prof. Hany Abdel-Malek,

Dr. Azza Rabie, Dr. Sameh Dakroury, Dr. Ahmed Abdel-Naby, and Eng. Ahmed El-Sharabasy, Faculty of Engineering, Cairo University, which have been reviewed in this chapter.

References

1. Abdel-Malek, H.L., Bandler, J.W.: Yield optimization for arbitrary statistical distributions: part I—theory. IEEE Trans. Circuits Syst. **27**, 245–253 (1980)
2. Abdel-Malek, H.L., Hassan, A.S.O.: The ellipsoidal technique for design centering and region approximation. IEEE Trans. Comput.-Aided Des. **10**, 1006–1014 (1991)
3. Abdel-Malek, H.L., Hassan, A.S.O., Bakr, M.H.: Statistical circuit design with the use of a modified ellipsoidal technique. Int. J. Microw. Millimeter Waves Comput.-Aided Eng. **7**, 117–129 (1997)
4. Abdel-Malek, H.L., Hassan, A.S.O., Bakr, M.H.: A boundary gradient search technique and its application in design centering. IEEE Trans. Comput.-Aided Des. **18**(11), 1654–1661 (1999)
5. Abdel-Malek, H.L., Hassan, A.S.O., Soliman, E.A., Dakroury, S.A.: The ellipsoidal technique for design centering of microwave circuits exploiting space-mapping interpolating surrogates. IEEE Trans. Microw. Theory Tech. **54**(10), 3731–3738 (2006)
6. Allen, P.E., Holberg, D.R.: CMOS Analog Circuit Design, 2nd edn. Oxford University Press, Oxford (2002)
7. Antreich, K.J., Graeb, H.E., Wieser, C.U.: Circuit analysis and optimization driven by worst-case distances. IEEE Trans. Comput.-Aided Des. **13**, 57–71 (1994)
8. Bakr, M.H., Bandler, J.W., Madsen, K., Søndergaard, J.: An introduction to the space mapping technique. Optim. Eng. **2**, 369–384 (2001)
9. Bandler, J.W., Abdel-Malek, H.L.: Optimal centering, tolerancing and yield determination via updated approximations and cuts. IEEE Trans. Circuits Syst. **25**, 853–871 (1978)
10. Bandler, J.W., Chen, S.H.: Circuit optimization: the state of the art. IEEE Trans. Microw. Theory Tech. **36**, 424–443 (1988)
11. Bandler, J.W., Seviora, R.E.: Computation of sensitivities for noncommensurate networks. IEEE Trans. Circuit Theory **CT-18**, 174–178 (1971)
12. Bandler, J.W., Zhang, Q.J., Song, J., Biernacki, R.M.: FAST gradient based yield optimization of nonlinear circuits. IEEE Trans. Microw. Theory Tech. **38**, 1701–1710 (1990)
13. Bandler, J.W., Biernacki, R.M., Chen, S.H., Grobelny, P.A., Hemmers, R.H.: Space mapping technique for electromagnetic optimization. IEEE Trans. Microw. Theory Tech. **42**, 2536–2544 (1994)
14. Bandler, J.W., Cheng, Q.S., Dakroury, S.A., Hailu, D.M., Madsen, K., Mohamed, A.S., Pedersen, F.: Space mapping interpolating surrogates for highly optimized EM-based design of microwave devices. In: IEEE MTT-S Int. Microwave Symp. Dig., Fort Worth, TX, vol. 3, pp. 1565–1568 (2004)
15. Bandler, J.W., Cheng, Q.S., Dakroury, S.A., Mohamed, A.S., Bakr, M.H., Madsen, K., Søndergaard, J.: Space mapping: the state of the art. IEEE Trans. Microw. Theory Tech. **52**, 337–361 (2004)
16. Broyden, C.G.: A class of methods for solving nonlinear simultaneous equations. Math. Comput. **19**, 577–593 (1965)
17. Cheng, Q.S., Bandler, J.W., Koziel, S., Bakr, M.H., Ogurtsov, S.: The state of the art of microwave CAD: EM-based optimization and modeling. Int. J. RF Microw. Comput.-Aided Eng. **20**, 475–491 (2010)
18. Conn, A.R., Toint, Ph.L.: An algorithm using quadratic interpolation for unconstrained derivative free optimization. In: Di Pillo, G., Giannes, F. (eds.) Nonlinear Optimization and Applications, pp. 27–47. Plenum Publishing, New York (1996)
19. Conn, A.R., Scheinberg, K., Toint, Ph.L.: A derivative free optimization algorithm in practice. In: Proceedings of 7th AIAA/USAF/NASA/ISSMO Symposium on Multidisciplinary Analysis and Optimization, St. Louis, MO (1998)

20. De Boor, C., Ron, A.: Computational aspects of polynomial interpolation in several variables. Math. Comput. **58**, 705–727 (1992)
21. De Klerk, E.: Aspects of Semidefinite Programming: Interior-Point Algorithms and Selected Applications. Kluwer Academic, New York (2002)
22. Director, S.W., Hachtel, G.D., Vidigal, L.M.: Computationally efficient yield estimation procedures based on simplicial approximation. IEEE Trans. Circuits Syst. **25**, 121–130 (1978)
23. Elias, N.J.: Acceptance sampling: an efficient accurate method for estimating and optimizing parametric yield. IEEE J. Solid-State Circuits **29**, 323–327 (1994)
24. Fortran90 Software Repository. http://www.nag.co.uk/nagware/examples.asp
25. Giunta, A.A., Wojtkiewicz, S.F. Jr., Eldred, M.S.: Overview of modern design of experiments methods for computational simulations. In: Proceedings of the 41st AIAA Aerospace Sciences Meeting and Exhibit, Reno, NV (2003). AIAA-2003-0649
26. Graeb, H.: Analog Design Centering and Sizing. Springer, Amsterdam (2007)
27. Hassan, A.S.O.: Normed distances and their applications in optimal circuit design. Optim. Eng. **4**, 197–213 (2003)
28. Hassan, A.S.O.: Design centering and region approximation via primal-dual interior-point technique. J. Eng. Appl. Sci. **51**(2), 195–212 (2004)
29. Hassan, A.S.O., Rabie, A.A.: Design centering using parallel-cuts ellipsoidal technique. J. Eng. Appl. Sci. **47**, 221–239 (2000)
30. Hassan, A.S.O., Abdel-Malek, H.L., Rabie, A.A.: Design centering and polyhedral region approximation via parallel-cuts ellipsoidal technique. Eng. Optim. **36**(1), 37–49 (2004)
31. Hassan, A.S.O., Abdel-Malek, H.L., Rabie, A.A.: None-derivative design centering algorithm using trust region optimization and variance reduction. Eng. Optim. **38**, 37–51 (2006)
32. Hassan, A.S.O., Mohamed, A.S., El-Sharabasy, A.Y.: Statistical microwave circuit optimization via a non-derivative trust region approach and space mapping surrogates. In: IEEE MTT-S Int. Microw. Symp. Dig., Baltimore, MD, USA (2011)
33. Hassan, A.S.O., Abdel-Naby, A.: A new hybrid method for optimal circuit design using semidefinite programming. Eng. Optim. 1–16 (2011)
34. Hocevar, D.E., Lightner, M.R., Trick, T.N.: A study of variance reduction techniques for estimating circuit yields. IEEE Trans. Comput.-Aided Des. **2**(3), 180–192 (1983)
35. Hocevar, D.E., Lightner, M.R., Trick, T.N.: An extrapolated yield approximation for use in yield maximization. IEEE Trans. Comput.-Aided Des. **3**, 279–287 (1984)
36. Keramat, M., Kielbasa, R.: A study of stratified sampling in variance reduction techniques for parametric yield estimations. IEEE Trans. Circuits Syst. II, Analog Digit. Signal Process. **45**(5), 575–583 (1998)
37. Koziel, S., Bandler, J.W., Madsen, K.: A space-mapping frame work for engineering optimization: theory and implementation. IEEE Trans. Microw. Theory Tech. **54**(10), 3721–3730 (2006)
38. Marcuvitz, N.: Waveguide Handbook, 1st edn. McGraw-Hill, New York (1951)
39. Matthaei, G.L., Young, L., Jones, E.M.T.: Microwave Filters, Impedance-Matching Networks, and Coupling Structures, 1st edn. McGraw-Hill, New York (1964)
40. McKay, M.D., Beckman, R.J., Conover, W.J.: A comparison of three methods for selecting values of input variables in analysis of output from a computer code. Technometrics **21**(2), 239–245 (1979)
41. Metropolis, N., Ulam, S.: The Monte-Carlo method. J. Am. Stat. Assoc. **44**, 335–341 (1949)
42. Moré, J.J., Sorensen, D.C.: Computing a trust region step. SIAM J. Sci. Stat. Comput. **4**(3), 553–572 (1983)
43. Powell, M.J.D.: UOBYQA. Unconstrained optimization by quadratic approximation. Math. Program. **92**, 555–582 (2002)
44. Powell, M.J.D.: The NEWUOA software for unconstrained optimization without derivatives. In: Di Pillo, G., Roma, M. (eds.) Large-Scale Nonlinear Optimization, pp. 255–297. Springer, New York (2006)
45. Powell, M.J.D.: Developments of NEWUOA for unconstrained minimization without derivatives. Technical Report, DAMTP 2007INA05, Department of Applied Mathematics and The-

oretical Physics, Cambridge University, UK (2007)
46. Sapatnekar, S.S., Vaidya, P.M., Kang, S.: Convexity-based algorithms for design centering. IEEE Trans. Comput.-Aided Des. **13**(12), 1536–1549 (1994)
47. Sauer, Th., Xu, Y.: On multivariate Lagrange interpolation. Math. Comput. **64**, 1147–1170 (1995)
48. Seifi, A., Ponnambalam, K., Vlach, J.: A unified approach to statistical design centering of integrated circuits with correlated parameters. IEEE Trans. Circuits Syst. **46**, 190–196 (1999)
49. Singhal, K., Pinel, J.F.: Statistical design centering and tolerancing using parametric sampling. IEEE Trans. Circuits Syst. **28**, 692–702 (1981)
50. Soliman, E.A., Bakr, M.H., Nikolova, N.K.: An adjoint variable method for sensitivity calculations of multiport devices. IEEE Trans. Microw. Theory Tech. **52**, 589–599 (2004)
51. Soliman, E.A.: Rapid frequency sweep technique for MoM planar solvers. IEE Proc. Microw. Antennas Propag. **151**, 277–282 (2004)
52. Soliman, E.A., Bakr, M.H., Nikolova, N.K.: Accelerated gradient-based optimization of planar circuits. IEEE Trans. Antennas Propag. **53**, 880–883 (2005)
53. Styblinski, M.A., Oplaski, L.J.: Algorithms and software tools for IC yield optimization based on fundamental fabrication parameters. IEEE Trans. Comput.-Aided Des. **5**, 79–89 (1986)
54. Toh, K.-C.: Primal-dual path-following algorithms for determinant maximization problems with linear matrix inequalities. Comput. Optim. Appl. **14**, 309–330 (1999)
55. Vandenberghe, L., Boyd, S., Wu, S.-P.: Determinant maximization with linear matrix inequality constraints. SIAM J. Matrix Anal. Appl. **19**, 499–533 (1998)
56. Vandenberghe, L., Boyd, S.: Applications of semidefinite programming. Appl. Numer. Math. **29**, 283–299 (1999)
57. Wojciechowski, J.M., Vlach, J.: Ellipsoidal method for design centering and yield estimation. IEEE Trans. Comput.-Aided Des. Integr. Circuits Syst. **12**, 1570–1579 (1993)
58. Wojciechowski, J., Opalski, L., Zantyniski, K.: Design centering using an approximation to the constraint region. IEEE Trans. Circuits Syst. **51**(3), 598–607 (2004)
59. Yu, T., Kang, S.M., Hajj, I.N., Trick, T.N.: Statistical performance modeling and parametric yield estimation of MOS VLSI. IEEE Trans. Comput.-Aided Des. **6**, 1013–1022 (1987)
60. Zaabab, A.H., Zhang, Q.J., Nakhla, M.: A neural network modeling approach to circuit optimization and statistical design. IEEE Trans. Microw. Theory Tech. **43**, 1349–1358 (1995)
61. Zhao, W., De, A., Donoro, D.G., Zhang, Y., Sarkar, T.K.: Antenna optimization by using NEWUOA. In: IEEE Antennas, Propag. Int. Symp., APSURSI 09 (2009)